

2020

## Development of a sensor suite for atmospheric boundary layer measurement with a small multicopter unmanned aerial system

Kevin A. Adkins

*Embry-Riddle Aeronautical University*, [kevin.adkins@erau.edu](mailto:kevin.adkins@erau.edu)

Christopher J. Swinford

*Embry-Riddle Aeronautical University*, [swinforc@my.erau.edu](mailto:swinforc@my.erau.edu)


Peter D. Wambolt

*Embry-Riddle Aeronautical University*, [wamboltp@my.erau.edu](mailto:wamboltp@my.erau.edu)

Gordon Bease

*FT Technologies*, [gordon.bease@fftech.co.uk](mailto:gordon.bease@fftech.co.uk)

Follow this and additional works at: <https://commons.erau.edu/ijaaa>

 Part of the [Atmospheric Sciences Commons](#), [Climate Commons](#), [Earth Sciences Commons](#), [Education Commons](#), [Engineering Commons](#), [Environmental Sciences Commons](#), [Meteorology Commons](#), and the [Other Oceanography and Atmospheric Sciences and Meteorology Commons](#)

### Scholarly Commons Citation

Adkins, K. A., Swinford, C. J., Wambolt, P. D., & Bease, G. (2020). Development of a sensor suite for atmospheric boundary layer measurement with a small multicopter unmanned aerial system. *International Journal of Aviation, Aeronautics, and Aerospace*, 7(1). Retrieved from <https://commons.erau.edu/ijaaa/vol7/iss1/4>

This Concept Paper is brought to you for free and open access by the Journals at Scholarly Commons. It has been accepted for inclusion in *International Journal of Aviation, Aeronautics, and Aerospace* by an authorized administrator of Scholarly Commons. For more information, please contact [commons@erau.edu](mailto:commons@erau.edu).

The lowest layer of the atmosphere, adjacent to the Earth's surface, is termed the atmospheric boundary layer (ABL). The ABL is a spatially and temporally dynamic region due to the influence of the Earth's surface. At this interface, exchanges of momentum, heat, water vapor, and radiant energy take place and are transported throughout the ABL by the mean wind and turbulence. Thus, the ABL plays a central role in both weather and climate and an improved understanding and representation of boundary layer processes will lead to better forecasting of weather and changes in climate. While many basic mechanisms of boundary layer processes are understood, there are many ABL features at fine temporal and spatial scales that are not fully understood. Instrumented small unmanned aerial systems (sUAS) afford a way to make high spatial resolution atmospheric measurements on-demand and, consequently, enable a more complete understanding of this region.

While examples exist of both in-situ and remote sensing sensors for ABL measurements, conventionally in-situ measurements have predominately been used for measurements requiring high accuracy and fine resolution. Although these in-situ sensors have been both manned aircraft-mounted and ground-based, sUAS hosted sensors maintain a unique advantage. Aircraft mounted sensors, including those mounted to both manned aircraft and free balloons, have the ability to cover vast horizontal and vertical distances in the ABL. However, manned aircraft are unable to safely operate at the lower portion of the ABL due to flight safety concerns and free balloons cannot be precisely controlled and, even when tethered, only offer skewed single column observations at best. Ground-based sensors, such as those attached to meteorological towers, are fixed, appreciably spaced, not easily moved and only offer insight into the lowest layer of the ABL. In contrast, an instrumented sUAS offers the ability to make on-demand measurements in a more continuous manner with high spatial resolution across vast horizontal and vertical distances, including at intermediate heights between the domains of ground-based sensors and manned aircraft operations.

### **Examples of sUAS as a Meteorological Sensing Platform**

Atmospheric observations using remote-controlled (R/C) aircraft took place as early as 1970 (Konrad, Hill, Rowland, & Meyer, 1970). More recently, sUAS have demonstrated the ability to acquire a wide range of atmospheric data using a variety of instruments. Solid-state temperature, pressure, and humidity sensors are readily hosted on a sUAS as long as their placement ensures that the measured environment is representative of the ambient atmosphere. Measurement of these scalar parameters have been made in a variety of investigations such as the characterization of the vertical structure of the ABL (Bonin, Chilson, Zielke, & Fedorovich, 2013; Lawrence & Balsley, 2013; Wainwright et al., 2015), the climate of the Arctic and Antarctic regions (Cassano, 2014; Knuth et al., 2013; Mayer,

Jonassen, Sandvik, & Reuder, 2012; Reuder, Brisset, Jonassen, Müller, & Mayer, 2008), the marine boundary layer (Cook, Strong, Garrett, & Marshall, 2013), surface fluxes (Reineman, Lenain, Statom, & Melville, 2013), sea breezes (Jonassen et al., 2015; Jonassen, Ólafsson, Águstsson, Rognvaldsson, & Reuder, 2012), changes to a wind turbine array boundary layer (WTABL) (Adkins & Sescu, 2017/2018), evaluation of ABL parameterizations for numerical weather prediction (NWP) (Mayer, Sandvik, Jonassen, & Reuder, 2012), and the monitoring of trace gases and aerosols (Broisy et al., 2017).

sUAS have also been used to make kinematic measurements. Cup and propeller anemometers are traditional mechanisms used to measure wind velocity. However, these instruments rely on their moving parts to come into dynamic equilibrium with the environment and are consequently unable to offer the fast response rate needed to capture the fluctuating component of the flow - i.e., turbulence. While a cup anemometer has been mounted on a sUAS for environmental sampling (Riddell, 2014), a cup anemometer's susceptibility to overspeed and sensitivity to the component of wind orthogonal to the plane of rotation makes it a poor choice for a sUAS wind measurement strategy (Barnard, 1992; Kaganov & Yaglom, 1976; Kirstensen, 1998). The strategies of deducing the wind velocity from the differential measurement of the power required from an unmanned aircraft (UA)'s motors (Marino et al., 2015) or comparison of the UA's inertial measurement unit (IMU) and global navigation satellite system (GNSS) (Bonin et al., 2013; Mayer et al., 2012; Reuder et al., 2008; Jonassen et al., 2012; Broisy et al., 2017; Balsley, Woodman, & Fritz, 2013; Neumann & Bartholmai, 2015; Palomaki, Rose, van den Bossche, Sherman, & De Wekker, 2017) negates the need for additional instrumentation but suffers from the same inability to finely resolve the wind vector.

Additionally, these strategies only provide insight into the horizontal components of the wind. Hot-wire anemometry offers an improved frequency response but the sensor's fragility is often incompatible with the forces experienced by an UA and requires frequent recalibration (Witte, 2016). Further, wind direction is not readily obtained unless more than one wire is used. Multi-hole pressure probes are a popular sensor choice for measuring wind velocity and fine-scale turbulence (Reuder, Jonassen, & Ólafsson, 2012; Witte, Singler, & Bailey, 2017; Yeung, Bramesfeld, Chung, & Foster, 2018). While the probe tips are susceptible to damage and possess a finite cone of acceptance for wind angles, the major drawback to their use on a hovering multirotor is their decreased accuracy for velocities below 3 m/s (Prudden et al., 2018). Alternatively, sonic anemometers overcome all of the aforementioned challenges by their use of immobile parts, a more robust construction, and a high measurement rate. In general, sonic anemometers determine the wind velocity by measuring the time-of-flight or, alternatively, the phase difference, brought about by the wind, of acoustic waves

and offer a more viable wind measurement strategy for multirotors. Their use on a fixed-wing UA (Reineman et al., 2013) has been shown to be in good agreement with ground-based measurement (Palomaki et al., 2017; Shimura, Inoue, Tsujimoto, Sasaki, & Iguchi, 2018).

### UAS Selection

A multirotor UA was chosen for its ability to hover and consequently provide flexibility in obtaining measurements in either a continuous manner or along a discontinuous trajectory at deliberately chosen points of interest. The ability to hover and fly a discontinuous trajectory allows the investigation of obstacle-laden environments, such as an urban environment. This strategy also ensures that the response time of any given sensor can be respected. Shown in Figure 1, the DJI S1000 octocopter was selected to host the suite of integrated sensors. The S1000 offers a stable platform, even with the loss of a rotor, and multiple mounting options. Additionally, with a predominately carbon fiber construction, the UA weighs approximately 4 kg but has a maximum takeoff weight (MTOW) of nearly 11 kg. Thus, it has a large payload capacity for this development project and those planned in the future. However, the sensor suite was developed to be UA agnostic by operating on an independent power source and not requiring any UA derived parameters. Therefore, this article focuses on the development of the sensor suite alone by first discussing the selection of the individual sensors and then the required system-level integration.

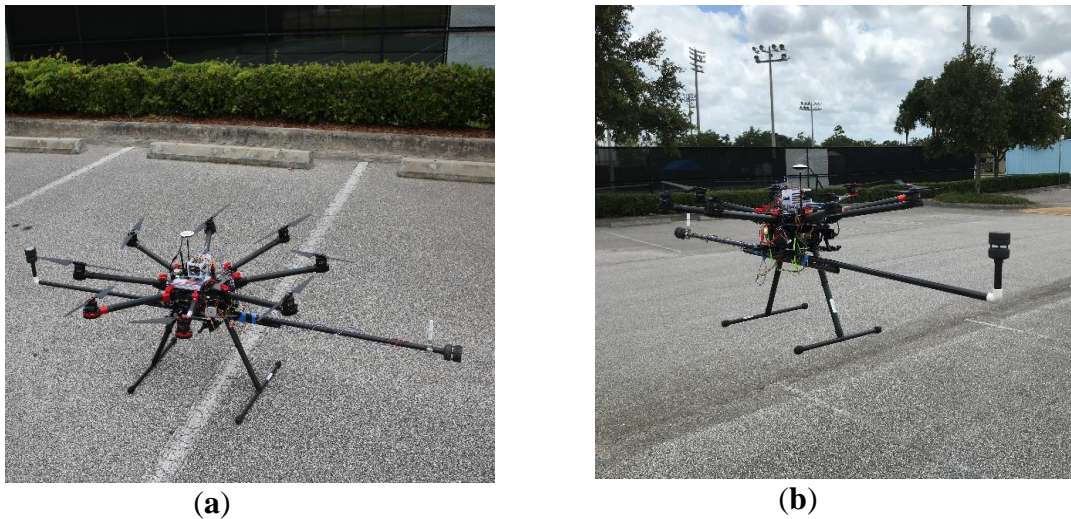


**Figure 1.** The fully instrumented unmanned aircraft. Microcontroller, power supply, data storage, and telemetry are centrally located with all meteorological instruments mounted on booms: (a) on the ground; (b) in the air.

## Sensors

Temperature, humidity, and wind speed, along with fluxes of momentum, heat, water vapor and radiant energy, are the parameters of greatest interest to boundary layer investigations. The selection of sensors was made with this in mind. The transport of heat, momentum and moisture in the ABL by the mean wind and turbulence lends itself to analysis by consideration of the respective mean value and a perturbation from it. For sensors that measure the turbulent fluctuation, a frequency response high enough to best capture the eddy scales germane to boundary layer processes drove the selection of the specific sensor model. Each sensor met the National Oceanic and Atmospheric Administration (NOAA) suggested guidelines for accuracy and range (Jacon, Axisa, Oncley, 2017) and are detailed below.

### Thermodynamic Sensors

Rotronic's HygroClip HC2A-S is used to measure both temperature and relative humidity. The HC2 system utilizes a resistance temperature detector (RTD) for temperature. Current is sent through a platinum element and the temperature is inferred from an accurate resistance-temperature relationship (Fraden, 2004). A capacitive humidity sensor is used for relative humidity. Constructed with two conductive plates separated by a dielectric material, as the dielectric absorbs moisture the capacitance increases and is correlated to humidity. The HC2A-S factors in temperature measurements from the RTD for relative humidity calculation (Rotronic, 2018). The requisite operating voltage of 3.3V to 5V allowed for the sensor to easily integrate with the Arduino Mega microcontroller. Rotronic's HygroClip HC2A-S comes factory calibrated and, prior to mounting, the integrity of the sensor was verified in an environmental test chamber. Complete performance specifications are given in Table 1.

**Table 1**  
*Specifications for the Rotronic's HygroClip HC2A-S*

Operating Range (Temperature)	-50 to 100° C
Operating Range (Humidity)	0 to 100%
Measuring Range (Temperature)	-40 to 60° C
Measuring Range (Humidity)	0 to 100 %
Accuracy (Temperature)	±0.1 K
Accuracy (Humidity)	±0.5 % RH
Operating Voltage	3.3 to 5 V
Output Rate	1 Hz

Barometric pressure is obtained from an ancillary onboard Pixhawk flight controller. With a range of 10 to 1200 mbar, the built-in barometer measures the atmospheric pressure with an accuracy of  $\pm 1.5$  mbar and a resolution of 0.01 mbar.

### **Kinematic Sensors**

The FT205 is a lightweight wind sensor which measures wind speed, wind direction and air temperature. Using Acoustic Resonance technology, a standing wave is resonated in the measurement cavity, resulting in an extremely high signal-to-noise (S/N) ratio, immune to vibrations and external acoustic noise. This is to the benefit of data quality and data availability. Wind speed and direction is discerned from the phase change of the acoustic signals and calculated independently of air pressure, temperature and humidity. The measurement cavity is designed to have a predictable and repeatable cosine response to inclined flow; therefore, two sensors, mounted orthogonally, and with signal outputs combined using sensor fusion, can inform the measurement of a 3-D wind field. The minimum operating voltage of the FT205 is 6 V, so the Arduino Mega output voltage is boosted by a voltage booster module to 22 V, within the operating range of the FT205. Sample rates are 10 Hz in either Continuous Update mode or Polled mode. The FT205 also features an integrated electronic compass. Complete performance specifications are given in Table 2.

**Table 2**

*Specifications for the FT Technologies FT205 Wind Sensor*

Wind Speed Range	0-75 m/s (0-145 kt)
Wind Speed Resolution	0.1 m/s
Wind Speed Accuracy	$\pm 0.3$ m/s (0-16 m/s) $\pm 2\%$ (16-40 m/s)
Wind Direction Range	0 to 360°
Wind Direction Resolution	1°
Wind Direction Accuracy	4° RMS
Operating Range (Temperature)	-20 to 70° C
Measuring Range (Temperature)	-20 to 60° C
Operating Range (Humidity)	0 to 100%
Operating Voltage	6 to 30 V
Output Rate	10 Hz



**Figure 2.** Pole mounted FT205 acoustic resonance wind sensor by FT Technologies that is used to measure horizontal (u,v) wind components.

### **System Integration**

#### **Atmospheric and Aircraft Sensors**

The scientific instrumentation system is comprised of two primary subsystems: an ancillary Pixhawk flight controller and the sensor suite (Figure 3). Measurements from each of these subsystems are brought together during post-processing by matching GPS time stamps on the data. A 3DR uBlox NEO-M8N GPS module is integrated with the Pixhawk while the sensor suite makes use of a 3DR uBlox LEA-6H GPS module. Each GPS module was configured in the uBlox uCenter software to output at a rate of 10Hz.



**Figure 3.** Pixhawk flight controller, sensor suite microcontroller, and telemetry.



The Arduino Mega is used to establish and control communication between all of the meteorological sensors using a Universal Asynchronous Receiver/Transmitter (UART). The Arduino Mega microcontroller provides the requisite serial communication ports and the required voltage and current for each of the system's components. For robustness, each component is securely soldered to the respective port using a custom-built proto-shield.

The ancillary Pixhawk 1 flight controller is mounted to the instrumentation shelf on the UA and provides the velocity and attitude of the UA using its built-in inertial measurement unit (IMU) and the paired GPS module. This allows for the creation of an extended Kalman filtered ground velocity that incorporates both GPS and IMU data and produces a velocity output at 10 Hz. This Kalman filtered velocity is subtracted from the wind sensor measurement and enables the calculation of an absolute wind measurement. Utilizing an ancillary IMU for this purpose, instead of referencing the UA's autopilot, allows the sensor suite to be completely UA agnostic and ensures portability in the future. The 9-axis IMU is capable of providing 3-axis accelerometer, magnetometer, and gyroscope measurements. These measurements ultimately provide the yaw, pitch, and roll of the aircraft, for coordinate transformation, to an accuracy of  $\pm 2^\circ$  and a resolution of  $0.01^\circ$  (ST Microelectronics, 2013). Calibration of the IMU was completed through the accompanying Mission Planner software.

### **Mounting**

While the idiosyncrasies of UA create a challenge for generalizing best practices for the mounting of instrumentation, established best practices for the hosting of meteorological instruments on tower, masts and booms were incorporated into the mounting of instrumentation, along with consideration of strategies that others have reported. To avoid any type of support structure shadowing, the anemometer measuring the vertical component of velocity ( $w$ ) (Figure 4) is mounted at the end of the extension boom. The sensor is mounted on the smallest diameter boom practical and has its outer diameter extending well outside of the boom's diameter. The RTD and hygrometer are mounted adjacent to this anemometer affording the calculation of vertical fluxes. While a minimum separation distance is desired for two sensors used in a flux measurement, a separation distance of three hygrometer diameters is incorporated to avoid contaminating the velocity measurement (Kaimel & Finnigan, 1994). The inboard mounting position of the RTD and hygrometer also takes into consideration the desired level of aspiration for the sensor without placing it too close to the rotors for compressional and frictional heating effects to be of concern (Jacob, Chilson, Houston, & Smith, 2018; Greene, Segales, Waugh, Duthoit, & Chilson, 2018). To enable the assumption that potential flow is being measured by the vertically-oriented anemometer measuring the horizontal components of velocity ( $u,v$ ) (Figure 2), the anemometer is mounted on an orthogonal member that extends



greater than three boom diameters away from the main boom and on the thinnest mast practical (Kaimel & Finnigan, 1994). The complete mount is crafted from carbon fiber for its superior strength-to-weight ratio and stiffness properties. The booms are attached to the UA's gimbal mount and thus take advantage of the mount's dampers. As a result, no vibration is observed in the extension booms during operation.



**Figure 4.** Boom mounted FT205 acoustic resonance wind sensor by FT Technologies that measures the vertical ( $w$ ) wind component, along with the adjacent mounting of the HygroClip HC2A-S for vertical flux calculations.

sUAS typically hover at 50 – 70% of their maximum available thrust (Prudden et al., 2018). Therefore, preliminary mount design took place by strapping the UA to a pole-mounted platform and mapping the airflow around its perimeter while maintaining thrust levels between 50 – 70%. The platform was vertically elevated greater than 5 UA diameters away from the ground to limit ground effect influences (Sanchez-Cuevas, Heredia et al., 2017). These tests were conducted inside and in the absence of any appreciable ambient flow and, consequently, the observed dimensions of the rotor-induced flow field were taken to be the worst-case scenario (Bruschia, Piotto, Dell'Agnello, Ware, & Roy, 2016). Complementing this testing, the UA was flown off an interior second floor balcony in a bank of theatrical fog. Both of these quantitative and qualitative tests indicated that the lateral extent of the rotor-induced flow field did not extend beyond 0.3 – 0.38 m away from the UA rotors. As a result, the sensors were mounted symmetrically on two horizontally oriented 1 m long carbon fiber booms that created nearly symmetrical lateral moments. These booms provided a mounting location that significantly exceeded the observed lateral dimensions of the rotor-induced flow field along with the area of influence observed by others (de

Boisblanc et al., 2014; Witte et al., 2017), including testing done by the sensor manufacturer. Following the mounting of all instrumentation in a finalized flight configuration, rotors on and off testing was accomplished, along with comparison to an adjacent surface-mounted anemometer. These tests validated that the UA accurately measures ambient wind speeds.

### **Data Collection, Storage, and Transmission**

Each of the two aforementioned sub-systems write and store data separately. Data collected by the sensor suite is stored in a comma delimited format on an integrated SD card module. Data gathered via the Pixhawk is stored within a binary log file on an internal micro-SD card within the flight controller. The binary log file is loaded into Pixhawk's Mission Planner and exported as a MATLAB file.

To enable informed real-time decision making during a flight, data packets containing the three wind velocity components (u,v,w), temperature, and humidity are telemetered to a ground station (GS) computer and parsed. This functionality empowers the scientific data team to observe current atmospheric conditions in a particular area and determine if additional time for investigation is warranted. To overcome any fears of data loss by dropped data packets, data used in post-processing is acquired from data locally written onboard the UA.

A 3DR radio telemetry (TM) module is used that offers a maximum data packet transfer rate of 250 kilobits per second, which far exceeds the data packet size being transferred by the sensor suite. The TM module operates over a frequency of 915 MHz and can transfer data over a range of approximately 300 m and at a 10 Hz rate.

### **Data Post-Processing**

Post-processing of the collected flight data aligns the data collected from the two isolated sub-systems. The data ingested into a MATLAB script from the Pixhawk is parsed into discrete slices using the GPS timestamp. The Kalman filtered velocity, roll, pitch, and yaw from the Pixhawk at any given moment is then matched to the timestamp associated with the three components of wind velocity, along with that of the temperature, pressure and humidity output from the sensor suite.

Data collected during flight is done so in a sensor frame of reference and must be subsequently converted to a body frame and ultimately to an Earth-fixed frame. The measured vector parameters,  $V_a$ , are transformed to the Earth frame,  $V_g$ , by the Euler angle rotation matrix represented in Equation 1, where pitch, roll, and yaw are given by  $\theta$ ,  $\phi$ ,  $\psi$  respectively. These transformations are accomplished through MATLAB's built-in matrix functions.

$$\begin{bmatrix} V_{x,g} \\ V_{y,g} \\ V_{z,g} \end{bmatrix} = \begin{bmatrix} \cos(\theta) \cos(\psi) & -\cos(\varphi) \sin(\psi) + \sin(\varphi) \sin(\theta) \cos(\psi) & \sin(\varphi) \sin(\psi) + \cos(\varphi) \sin(\theta) \cos(\psi) \\ \cos(\theta) \sin(\psi) & \cos(\varphi) \cos(\psi) + \sin(\varphi) \sin(\theta) \cos(\psi) & -\sin(\varphi) \cos(\psi) + \cos(\varphi) \sin(\theta) \cos(\psi) \\ -\sin(\theta) & \sin(\varphi) \cos(\theta) & \cos(\varphi) \cos(\theta) \end{bmatrix} \begin{bmatrix} V_{x,a} \\ V_{y,a} \\ V_{z,a} \end{bmatrix} \quad (1)$$

Again, since the UA is moving, even while working to maintain position in a hover, the vehicle's motion must be subtracted from the wind sensor measurement in order to obtain an absolute measurement of the wind velocity. Data from the Pixhawk's IMU and interfaced GPS module is blended into a Kalman filtered velocity that is used to remove the UA's motion from the wind sensed by the anemometers.

### Conclusions

Compared to traditional measurement strategies, a sUAS affords many advantages in the measurement of ABL thermodynamic and kinematic variables. Compared to a fixed-wing UA, a multirotor, with its maneuverability and ability to hover, additionally affords the opportunity to explore a greater number of locations within an obstacle-laden environment and obtain temporal changes at a fixed-location. However, sensor selection must consider the specific measurement goals and the rotor-induced flow field around a multirotor provides distinct measurement challenges. Following careful selection of sensors and quantitative and qualitative observations of the rotor-induced flow field, a sensor suite was developed for the measurement and telemetering of temperature, humidity, and pressure, along with measurement of the 3 components of velocity, including in a hover. This platform is geared for investigation of the ABL, including the WTABL and the urban boundary layer. Future enhancements include complete onboard post-processing and an increase in the telemetering range.

### References

- Adkins, K. A., & Sescu, A. (2017). Observations of relative humidity in the near-wake of a wind turbine using an instrumented unmanned aerial system. *International Journal of Green Energy*, 14(10), 845-860. doi:10.1080/15435075.2017.1334661
- Adkins, K. A., & Sescu, A. (2018). Analysis of near-surface relative humidity in a wind turbine array boundary layer using an instrumented unmanned aerial system and large-eddy simulation. *Wind Energy*, 21(11), 1155-1168. doi:10.1002/we.2220
- Balsley, B., Lawrence, D., Woodman, R., & Fritts, D. (2013). Fine-scale characteristics of temperature, wind, and turbulence in the lower atmosphere (0–1,300m) over the South Peruvian coast. *Boundary-Layer Meteorology*, 147, 165–178. doi:10.1007/s10546-012-9774-x
- Barnard, J. C. (1992). *Comparison of anemometers for turbulence characterization*. Wind power 1992 Conference. Retrieved from <https://www.osti.gov/servlets/purl/7092648>
- Bonin, T., Chilson, P., Zielke, B., & Fedorovich, E. (2013). Observations of the early evening boundary-layer transition using a small unmanned aerial system. *Boundary-Layer Meteorology*, 146, (1), 119–132. doi:10.1007/s10546-012-9760-3
- Brosy, C., Krampf, K., Zeeman, M., Wolf, B., Junkermann, W., Schäfer, K., Emeis, S., & Kunstmann, H. (2017). Simultaneous multicopter-based air sampling and sensing of meteorological variables. *Atmospheric Measurement Techniques*, 10(8), 2773-2784. doi:10.5194/amt-10-2773-2017
- Bruschia, P., Piotta, M., Dell’Agnello, F., Ware, J., & Roy, N. (2016). Wind speed and direction detection by means of solid-state anemometers embedded on small quadcopters. *Procedia Engineering*, 168, 802-805. doi.org/10.1016/j.proeng.2016.11.274
- Cassano, J. J. (2014). Observations of atmospheric boundary layer temperature profiles with a small unmanned aerial vehicle. *Antarctic Science*, 26(2), 205–213. doi:10.1017/S0954102013000539
- Cook, D. E., Strong, P. A., Garrett, S. A., & Marshall, R. E. (2013). A small unmanned aerial system (UAS) for coastal atmospheric research: Preliminary results from New Zealand. *Journal of the Royal Society of New Zealand*, 43(2), 108–115. doi:10.1080/03036758.2012.695280
- de Boisblanc, I., Dodbele, N., Kussmann, L., Mukherji, R., Chestnut, D., Phelps, S., Lewin, G. C., & de Wekker, S. (2014). *Designing a hexacopter for the collection of atmospheric flow data*. Paper presented at the 2014 Systems and Information Engineering Design Symposium, 147-152. doi:10.1109/SIEDS.2014.6829915

- Fraden, J. (2004). *Handbook of modern sensors: Physics, designs, and applications (3rd ed.)*. San Diego, CA: Springer-Verlag.
- Greene, B. R., Segales, A. R., Waugh, S., Duthoit, S., & Chilson, P. B. (2018). Considerations for temperature sensor placement on rotary-wing unmanned aircraft systems. *Atmospheric Measurement Techniques*, 11(10), 5519-5530. doi:10.5194/amt-11-5519-2018
- Jacob, J., Axisa, A., & Oncley, S. (2017). *Unmanned aerial systems for atmospheric research: Instrumentation issues for atmospheric measurements*. NCAR/EOL Community Workshop on Unmanned Aerial Systems for Atmospheric Research.
- Jacob, J., Chilson, P., Houston, A., & Smith, S. (2018). Considerations for atmospheric measurements with small unmanned aircraft systems. *Atmosphere*, 9(7), 252. doi:10.3390/atmos9070252
- Jonassen, M. O., Ólafsson, H., Ágústsson, H., Rognvaldsson, O., & Reuder, J. (2012). Improving high resolution numerical weather simulations by assimilating data from an unmanned aerial system. *Monthly Weather Review*, 140(11), 3734–3756. doi:10.1175/MWR-D-11-00344.1
- Jonassen, M., O., Tisler, P., Altstädter, B., Scholtz, A., Vihma, T., Lampert, A., König-Langlo, G., & Lüpkes, C. (2015). Application of remotely piloted aircraft systems in observing the atmospheric boundary layer over Antarctic sea ice in winter. *Polar Research*, 34, 25651. doi:10.3402/polar.v34.25651
- Kaganov, E. I., & Yaglom, A. M. (1976). Errors in wind-speed measurements by rotation anemometers. *Boundary Layer Meteorology*, 15-34. Springer Netherlands.
- Kaimal, J. C., & Finnigan, J. J. (1994). *Atmospheric boundary layer flows: Their structure and measurement*. New York, NY: Oxford University Press.
- Kirstensen, L. (1998). Cup anemometer behavior in turbulent environments. *Journal of Atmospheric and Oceanic Technology*, 5-17.
- Knuth, S. L., Cassano, J. J., Maslanik, J. A., Herrmann, P. D., Kernebone, P. A., Crocker, R. I., & Logan, N. J. (2013). Unmanned aircraft system measurements of the atmospheric boundary layer over terra nova bay, Antarctica. *Earth System Science Data*, 5(1), 57-69. doi:10.5194/essd-5-57-2013.
- Konrad, T. G., Hill, M. L., Rowland, J. R., & Meyer, J. H. (1970). A small, radio-controlled aircraft as a platform for meteorological sensors. *Johns Hopkins APL Tech Digest*, 10, 11–19.
- Lawrence, D. A., & Balsley, B. B. (2013). High-resolution atmospheric sensing of multiple atmospheric variables using the datahawk small airborne measurement system. *Journal of Atmospheric & Oceanic Technology*, 30(10), 2352–2366. doi:10.1175/JTECH-D-12-00089.1

- Marino, M., Fisher, A., Clothier, R., Watkins, S., Prudden, S., & Leung, C. S. (2015). An evaluation of multi-rotor unmanned aircraft as flying wind sensors. *International Journal of Micro Air Vehicles*, 7(3), 285-299. doi:10.1260/1756-8293.7.3.285
- Mayer, S., Jonassen, M., Sandvik, A., & Reuder, J. (2012). Profiling the arctic stable boundary layer in advent valley, svalbard: measurements and simulations. *Boundary-Layer Meteorology*, 143(3), 507–526. doi:10.1007/s10546-012-9709-6
- Mayer, S., Sandvik, A., Jonassen, M., & Reuder, J. (2012). Atmospheric profiling with the UAS sumo: A new perspective for the evaluation of fine-scale atmospheric models. *Meteorology & Atmospheric Physics*, 116(1,2), 15–26. doi:10.1007/s00703-010-0063-2
- Neumann, P. P., & Bartholmai, M. (2015). Real-time wind estimation on a micro unmanned aerial vehicle using its inertial measurement unit. *Sensors & Actuators: A. Physical*, 235, 300-310. doi:10.1016/j.sna.2015.09.036
- Palomaki, R. T., Rose, N. T., van den Bossche, M., Sherman, T. J., & De Wekker, S. F. J. (2017). Wind estimation in the lower atmosphere using multirotor aircraft. *Journal of Atmospheric and Oceanic Technology*, 34(5), 1183-1191. doi:10.1175/JTECH-D-16-0177.
- Prudden, S., Fisher, A., Marino, M., Mohamed, A., Watkins, S., & Wild, G. (2018). Measuring wind with small unmanned aircraft systems. *Journal of Wind Engineering & Industrial Aerodynamics*, 176, 197-210. doi:10.1016/j.jweia.2018.03.029
- Reineman, B. D., Lenain, L., Statom, N. M., & Melville, W. K. (2013). Development and testing of instrumentation for UAV-based flux measurements within terrestrial and marine atmospheric boundary layers. *Journal of Atmospheric & Oceanic Technology*, 30(7), 1295–1319. doi:10.1175/JTECH-D-12-00176.1
- Reuder, J., Brisset, P., Jonassen, M., Müller, M., & Mayer, S. (2008). Sumo: A small unmanned meteorological observer for atmospheric boundary layer research. *IOP Conference Series: Earth & Environmental Science*, 1(1),1.
- Reuder, J., Jonassen, M., & Ólafsson, H. (2012). The small unmanned meteorological observer sumo: Recent developments and applications of a Micro-UAS for atmospheric boundary layer research. *ActaGeophysica*, 60(5), 1454. doi:10.2478/s11600-012-0042-8
- Riddell, K. D. A. (2014). *Design, testing and demonstration of a small unmanned aircraft system (sUAS) and payload for measuring wind speed and particulate matter in the atmospheric boundary layer* (Order No. 1569498). Available from ProQuest Dissertations & Theses Global. (1629019034). Retrieved from

- <http://search.proquest.com.ezproxy.libproxy.db.erau.edu/docview/1629019034?accountid=27203>.
- Rotronic. (2018). *The capacitive humidity sensor – How it works & attributes of the uncertainty budget*. Retrieved from [https://www.rotrotron.com/media/productattachments/files/c/a/capacitive\\_humidity\\_sensor\\_final.pdf](https://www.rotrotron.com/media/productattachments/files/c/a/capacitive_humidity_sensor_final.pdf)
- Sanchez-Cuevas, P., Heredia, G., & Ollero, A. (2017). Characterization of the aerodynamic ground effect and its influence in multirotor control. *International Journal of Aerospace Engineering*, 1-17. doi:10.1155/2017/1823056.
- Shimura, T., Inoue, M., Tsujimoto, H., Sasaki, K., & Iguchi, M. (2018). Estimation of wind vector profile using a hexarotor unmanned aerial vehicle and its application to meteorological observation up to 1000 m above surface. *Journal of Atmospheric and Oceanic Technology*, 35(8), 1621-1631.
- ST Microelectronics. (2013, November) *Ultra-compact high-performance eCompass module: 3D accelerometer and 3D magnetometer*. LSM303D datasheet. Retrieved from <https://www.st.com/resource/en/datasheet/lsm303dlhc.pdf>
- Wainwright, C., Bonin, T., Chilson, P., Gibbs, J., Fedorovich, E., & Palmer, R. (2015). Methods for evaluating the temperature structure-function parameter using unmanned aerial systems and large-eddy simulation. *Boundary-Layer Meteorology*, 155(2), 189–208. doi:10.1007/s10546-014-0001-9
- Witte, B. (2016). *Development of an unmanned aerial vehicle for atmospheric turbulence measurement*. Theses and Dissertations--Mechanical Engineering, 82. [https://uknowledge.uky.edu/me\\_etds/82](https://uknowledge.uky.edu/me_etds/82).
- Witte, B., Singler, R., & Bailey, S. (2017). Development of an unmanned aerial vehicle for the measurement of turbulence in the atmospheric boundary layer. *Atmosphere*, 8(12), 195. doi:10.3390/atmos8100195
- Yeung, A., Bramesfeld, G., Chung, J., & Foster, S. (2018). Measuring low-altitude wind gusts using the unmanned aerial vehicle GustAV. *Journal of Unmanned Vehicle Systems*, 6(4), 235-248. doi:10.1139/juvs-2017-0029